Dyes and Pigments 87 (2010) 69–75

Contents lists available at ScienceDirect

Dyes and Pigments

journal homepage: www.elsevier.com/locate/dyepig

The preparation and optical limiting properties of POSS-based molecular hybrid functional materials

Xinyan Su [a], Shanyi Guang [a], Hongyao Xu [a,c,*], Junyi Yang [b], Yinglin Song [b]

[a] College of Material Science and Engineering & State Key Laboratory for Modification of Chemical Fibers and Polymer Materials, Donghua University, Shanghai 201620, China
[b] Department of Physics, Suzhou University, Suzhou 215008, China
[c] State Key Laboratory of Crystal Material, Shandong University, Jinan 250100, China

ARTICLE INFO

Article history:
Received 1 December 2009
Received in revised form
24 February 2010
Accepted 26 February 2010
Available online 4 March 2010

Keywords:
Organic/inorganic hybrid
POSS
NLO
Optical limiting
Thermal stability
Azobenzene

ABSTRACT

A series of organic/inorganic molecular hybrid nonlinear optical materials were prepared by incorporating azobenzene nonlinear optical chromophores into nanosized, inorganic, polyhedral oligomeric silsesquioxane. Each of the hybrids was soluble in common solvents such as $CHCl_3$, THF, toluene and $C_2H_4Cl_2$, and exhibited good film-forming properties. Their structures and properties were characterized using FTIR, ^{1}H NMR, ^{13}C NMR, ^{29}Si NMR, UV, TGA, DSC and nonlinear optical analyses, respectively. All hybrid compounds displayed good optical limiting properties, large nonlinear optical response and high thermal stability. The optical limiting mechanism was investigated.

1. Introduction

π-Electron conjugated, organic optical limiting materials have attracted significant attention in recent years owing to the growing needs for protection of both optical sensitive devices and the human eye from laser damage, owing to their large and rapid nonlinear optical response [1,2]. Although many organic and polymeric optical limiting materials have been investigated [3–13], these materials often posess poor solubility and low thermal stability due to the highly conjugated, rigid structure of the chromophores. To improve the thermal properties of organic optical materials, organic–inorganic hybrid materials combine the properties of traditional organic materials (i.e. ease of molecular design and low cost) with those of inorganic compounds (i.e. high thermal and oxidative stability) [14,15].

A typical hybrid material normally contains an inorganic phase bonded (often covalently) with an organic phase; however, the major challenge lies in how to bind an organic compound covalently with inorganic moieties during synthesis. The discovery of polyhedral oligomeric silsesquioxane (POSS) overcomes this synthetic difficulty. POSS is a nanoscale, cage-like molecule that has a well-defined cube-like inorganic core (Si_8O_{12}) surrounded by eight organic corner groups (functional or inert) and which provides an excellent platform for nanotechnology applications and novel molecular hybrids due to its perfectly defined spatial geometry [16]. By incorporating POSS cages into organic molecules or polymers, POSS-based functional materials have been prepared that display superior properties to the organic material alone [17–23]. The present research group has developed a series of POSS-based hybrid materials and reported that these hybrid materials have high thermal properties and good solubility [14,24–27]. However, POSS-based hybrid optical limiting materials have received less attention [28,29].

In this work, a series of star-like molecular hybrid functional materials from multi functional POSS ($\mathbf{T_8^H}$) was prepared. Their structures and properties were characterized and evaluated. The relationship between the structure and properties was investigated in detail.

2. Experimental

2.1. Materials and instruments

Octahydridosilsesquioxane [$(HSiO_{1.5})_8$, $\mathbf{T_8^H}$] was synthesized according to the procedures described in [30]. The synthesis and

* Corresponding author. College of Material Science and Engineering & State Key Laboratory for Modification of Chemical Fibers and Polymer Materials, Donghua University, Shanghai 201620, China. Tel./fax: +86 21 67792874.
E-mail address: hongyaoxu@163.com (H. Xu).

0143-7208/$ – see front matter © 2010 Elsevier Ltd. All rights reserved.
doi:10.1016/j.dyepig.2010.02.006

characterization of the azobenzene chromophores 1-(4-methoxyphenyl)-2-(4-(prop-2-ynyloxy)phenyl)diazene (**M1**), 4-((4-methoxyphenyl)diazenyl)phenyl 4-(prop-2-ynyloxy)benzoate (**M2**) and N-(4-((4-(prop-2-ynyloxy)phenyl)diazenyl)phenyl)dodecanamide (**M3**) were described previoulsy [11]. All chromophores are linked with a terminal alkynyl bond as the active reactive group. **P1**–**P3** were prepared by hydrosilylation of **M1**–**M3** and POSS ($\mathbf{T_8^H}$), as shown in Scheme 1. The platinum dicyclopentadiene complex, [Pt(dcp)], was synthesized according to the literature procedure [31] and was used as a 2 mM solution in $C_2H_4Cl_2$. The platinum divinyltetramethyldisiloxane complex, Pt(dvs), was obtained from PCR Co. and diluted to a 2 mM solution in distilled toluene before use. $C_2H_4Cl_2$ for hydrosilylation reaction was distilled from CaH_2 under N_2.

FTIR spectra were measured with a Nicolet NEXUS 870 FTIR spectrophotometer using KBr powder at room temperature. ^{1}H NMR, ^{13}C NMR and ^{29}Si NMR spectra were recorded on a Bruker DMX-400 spectrometer using chloroform-d ($CDCl_3$). Weight–average (M_w) and number–average (M_n) molecular weights and polydispersity index (PDI, M_w/M_n) were determined by a Waters 515 gel permeation chromatograph (GPC). Differential scanning calorimetry (DSC) was performed on a DSC 9000 equipped with a liquid nitrogen cooling accessory (LNCA) unit under a continuous nitrogen purge (50 mL/min). The scan rate was 10 °C/min within the temperature range 40–300 °C. Thermogravimetric analysis (TGA) was carried out using a TGA 2050 thermogravimetric analyzer with a heating rate of 10 °C/min from 25 to 700 °C under a continuous nitrogen purge (100 mL/min). The thermal degradation temperature (T_d) was defined as the temperature of 5% weight loss. UV spectra were recorded on a Shimadzu UV-265 spectrometer.

The nonlinear absorption properties of the samples were performed by open *Z*-scan technique with a frequency doubled, Q-switched, mode-locked Continuum ns/ps Nd:YAG laser system, which provides linearly polarized 4 ns optical pulses at 532 nm wavelength with a repetition of 1 Hz. The experiment was set up as in the literature [32]. The solution sample was contained in a 2 mm quartz cell. The input energy was 62 μJ. The radius ω_0 at beam waist was 50 mm. The samples were moved along the axis of the incident beam (*z* direction).

The investigation of the optical limiting properties of the samples was carried out by using the same laser system as in the nonlinear absorption experiment. The experimental arrangement is similar with that in the literature [33]. The samples were housed in quartz cells with a path of 2 mm. The input laser pulses adjusted by an attenuator (Newport) were split into two beams. One was employed as a reference to monitor the incident laser energy, and the other was focused onto the sample cell by using a lens with a 300 mm focal length. The samples were positioned at the focus. The incident and transmitted laser pulses were monitored by two energy detectors, D1 and D2 (Rjp-735 energy probes, Laser Precision).

2.2. Synthesis

The hydrosilylation reactions and manipulations for preparing molecular hybrid materials were carried out under N_2 protection using a vacuum-line system. The hybrids **P1**, **P2** and **P3** (all feed ratio of monomers to $\mathbf{T_8^H}$ are at 8:1) were prepared using a conventional Pt (dcp) catalyst addition reaction (Scheme 1). A typical procedure is: 5 mL $C_2H_4Cl_2$, 21.2 mg (0.05 mmol) octahydridosilsesquioxane, 1.0 mg Pt(dcp) and 0.11 g (0.4 mmol) 1-(4-methoxyphenyl)-2-(4-(prop-2-ynyloxy)-phenyl)diazene (**M1**) were added to a 20 mL Schlenk tube equipped with side arm. The mixture was stirred at 80 °C for 10 h; after cooling to room temperature, the mixture was poured into 200 mL hexane with vigorous agitation to dissolve the unreacted parts and to precipitate the product. The precipitate was centrifuged and redissolved in a minimum of THF. The ensuing THF solution was added dropwise to 200 mL hexane so as to precipitate the compound once again. This dissolution–precipitation process was repeated three times and the final isolated precipitate was dried under vacuum at 80 °C to constant mass; the yellow powder **P1** was obtained. Yield: 54.1%. M_n = 2250, PDI, 1.02 (GPC, polystyrene). FTIR (KBr, cm^{-1}): 3071 (=C–H), 2923, 2838 (CH_3), 2264 (Si–H), 1599 (C=C), 1251 (C–O–C), 1110 (Si–O–Si), 840 (p-Ar). ^{1}H NMR (400 MHz, $CDCl_3$): δ 7.80 (br, Ar–H), 6.94 (br, Ar–H), 6.10 (br, C*H* = CHSi β-*trans*), 5.94 (br, CH = C*H*Si β-*trans* and CH_2 = C–Si α), 4.67 (br, OCH_2), 4.28 (Si–H), 3.87 (br, OCH_3). ^{13}C NMR (75 MHz, $CDCl_3$): δ 161.3, 160.2, 146.8, 131.3, 124.5, 114.9, 114.2, 69.0, 55.5. ^{29}Si NMR ($CDCl_3$, 79.5 MHz, ppm): δ −79.12 (Si–C β-*trans*), −81.15 (Si–C α), −83.69 (Si–H).

P2: Yellow powder. Yield: 51.3%. *M*n = 3610, PDI, 1.02 (GPC, polystyrene). FTIR (KBr, cm^{-1}): 3071 (=C–H), 2929, 2838 (CH_3), 2264 (Si–H), 1734 (C=O), 1603 (C=C), 1254 (C–O–C), 1107 (Si–O–Si), 841 (p-Ar). ^{1}H NMR (400 MHz, $CDCl_3$): δ 8.07, 7.87 (br, Ar–H), 6.90 (br, Ar–H), 6.11 (br, C*H*=CHSi β-*trans*), 5.97 (br, CH=C*H*Si β-*trans* and CH_2=C–Si α), 4.70 (br, OCH_2,), 4.26(s, Si–H), 3.88 (br, OCH_3). ^{13}C NMR (75 MHz, $CDCl_3$): δ 164.3, 162.0, 152.4, 150.3, 146.9, 132.3, 124.8, 123.7, 122.3, 114.6, 114.2, 98.1, 70.3 (OCH_2), 55.5 (OCH_3). ^{29}Si NMR ($CDCl_3$, 79.5 MHz, ppm): δ −80.01 (Si–C β-*trans*), −81.62 (Si–C α), −83.51 (Si–H).

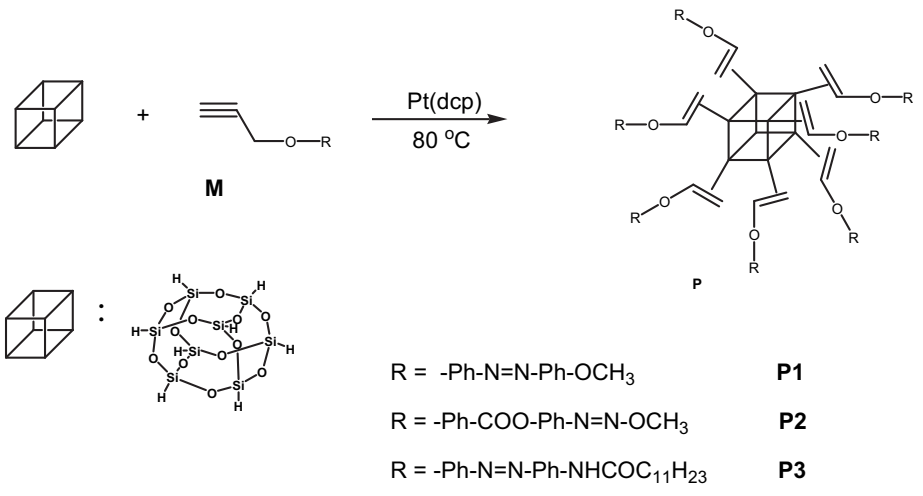

Scheme 1. Synthetic routes to the hybrids.

P3: brown powder. Yield: 47.6%. *M*n = 3740, PDI, 1.24 (GPC, polystyrene). FTIR(KBr, cm^{-1}): 3415 (N–H), 3050 (C=C–H); 2924, 2853(CH_3, CH_2), 2264 (Si–H), 1663 (C=O); 1598, 1499 (Ar); 1246 (C–O–C); 1137 (Si–O–Si); 883 (Si–H, in-plane bending), 843 (p-Ar). ^{1}H NMR (400 MHz, $CDCl_3$): δ 7.38–7.91 (br, N*H*, Ar–H), 6.74–7.10 (br, Ar–H and cis olefin), 5.97–6.12 (br, CH=C*H*Si β-*trans* and CH_2=C–Si α), 4.64, 4.79 (br, OCH_2), 4.27 (br, Si–H), 2.38 (br, CH_2CONH), 1.73 (br, CH_2CH_2CONH), 1.24 (br, $CH_3(CH_2)_8$), 0.87 (br, CH_3). ^{13}C NMR (75 MHz, $CDCl_3$): δ 171.8, 159.6, 148.9, 147.0, 140.1, 130.9, 124.5, 123.6, 119.8, 115.1, 114.9, 70.1 (OCH_2), 69.4 (OCH_2), 37.8, 31.9, 29.7–29.4, 25.7, 22.7, 14.1. ^{29}Si NMR ($CDCl_3$, 79.5 MHz, ppm): δ −79.81 (Si–C β-*trans*), −81.52 (Si–C α), −83.75 (Si–H).

3. Results and discussions

3.1. Structural characterization

Fig. 1 shows the FTIR spectra of POSS ($\mathbf{T_8^H}$), **M3** and hybrid **P3**. Monomer **M3** shows characteristic ≡C–H, C≡C and C=O stretching vibration at 3290, 2133, and 1665 cm^{-1}, respectively. $\mathbf{T_8^H}$ displays characteristic bands at 2292 and 1130 cm^{-1}, which are assigned to the Si–H and Si–O–Si stretching vibration absorption, respectively. The acetylene characteristic absorption bands of **M3** at 3290 and 2133 cm^{-1}, and Si–H characteristic absorption band of POSS at 2292 cm^{-1} completely disappear in the spectrum of **P3**. However, C=O at 1663 cm^{-1} and Si–O–Si at 1130 cm^{-1} stretching vibration still emerge in the FTIR spectrum of **P3**. Simultaneously, the relative intensity of the C=C absorption band at 1598 cm^{-1} (vs C=O stretching band at 1663 cm^{-1}) significantly increases and a new vibration band at 1508 cm^{-1} assigning to Si–C vibration absorption also appears in the FTIR spectrum of **P3**, indicating that hydrosilylative addition reaction between the Si–H groups of cube-like POSS and azobenzene-containing acetylene has happened and azobenzene acetylene has been incorporated into POSS cage to form POSS-containing molecular hybrids. Similar results also were found in the spectra of **P1** and **P2**.

These hybrids are completely soluble in common organic solvents such as $CHCl_3$, toluene, THF and 1,2-dichloroethane etc. Thus, their structures can be characterized by solution spectral method. Fig. 2 displays the ^{1}H NMR spectra of **M3**, $\mathbf{T_8^H}$, and **P3** in $CDCl_3$. $\mathbf{T_8^H}$ shows a characteristic proton absorption band at 4.25 ppm assigning to Si–H and **M3** possesses a characteristic acetylene proton resonance absorption band at δ 2.56 ppm.

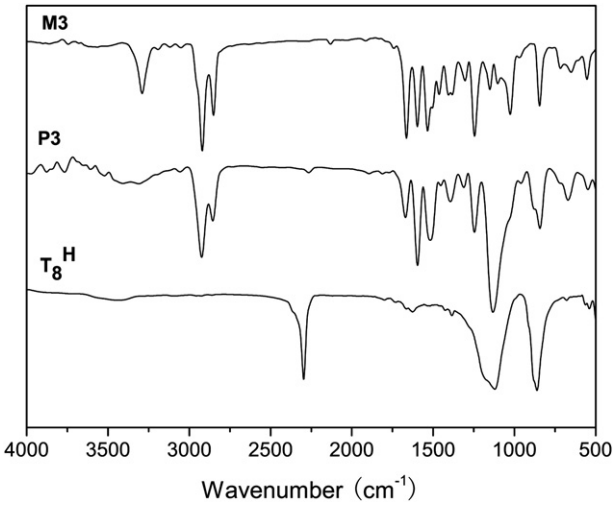

Fig. 1. IR spectra of $\mathbf{T_8^H}$, **M3** and **P3**.

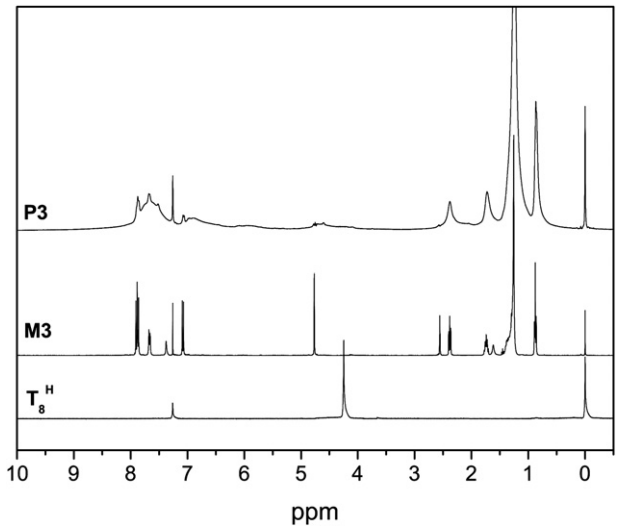

Fig. 2. ^{1}H NMR spectra of $\mathbf{T_8^H}$, **M3** and **P3** in $CDCl_3$.

However, the characteristic absorption of the acetylene proton at δ 2.56 ppm and Si–H proton absorption at 4.25 ppm almost completely disappear and a new broad characteristic absorption peaks at δ 6.12–5.97 ppm corresponding to the CH_2=C–Si (α-addition hybrids) and C*H*=C*H*–Si (β-addition hybrids) appears in the ^{1}H NMR spectrum of hybrid **P3**, further indicating that C≡C has changed into C=C group, and the star-type hybrid has been synthesized successfully by hydrosilylation reaction. This is consistent with that of FTIR speactra. Similar phenomena were observed in the ^{1}H NMR spectra of **P2** and **P3**.

Fig. 3 shows the ^{13}C NMR spectrum of **M3** and **P3**. The acetylene carbon atoms of **M3** absorbs at δ 78.1 and 75.9 ppm, these peaks completely disappear in the spectrum of **P3** and two new peaks at δ 69.4 and 70.1 ppm assigning to ethylene carbon of OCH_2C=C appear in the spectrum of **P3**, further confirming that azobenzene acetylenes have reacted with POSS.

Fig. 4 gives the ^{29}Si NMR spectra of **P3** and $\mathbf{T_8^H}$. It can be seen from Fig. 4 that two new peaks at −79.81 (β-*trans*, Si–C=) and −81.52 (α, Si–C=) assigning to α and β-adducts appear in the spectrum of **P3**, further supporting that the star-type hybrid has been prepared successfully by hydrosilylation reaction.

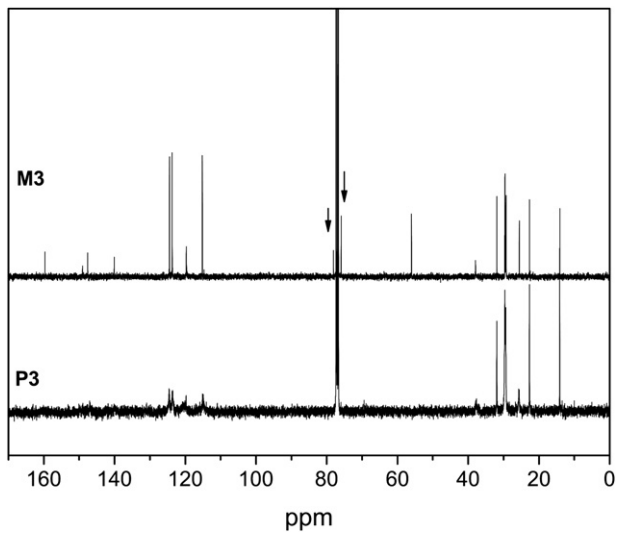

Fig. 3. ^{13}C NMR spectra of **M3** and **P3** in $CDCl_3$.

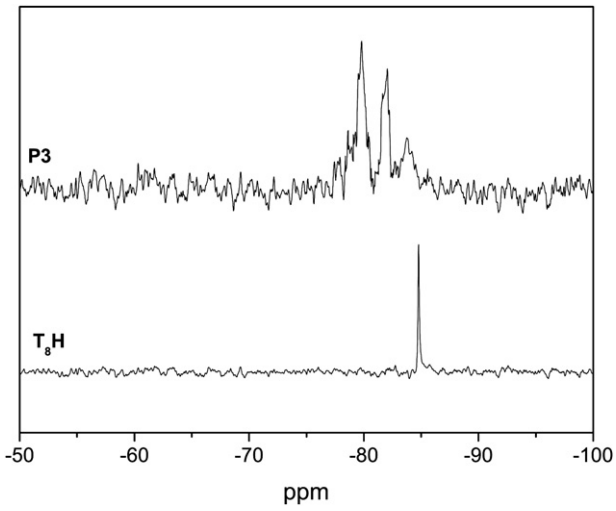

Fig. 4. ^{29}Si NMR spectra of $\mathbf{T_8^H}$ and **P3** in $CDCl_3$.

3.2. Absorption spectra of the hybrids

Fig. 5A shows the normalized UV–vis absorption spectra of **P1**, **P2**, **P3** and **M3** in dilute (10^{-5} M) THF solutions. From Fig. 5A it can be seen that **P3** and **M3** display nearly the same maximum absorption wavelength and spectral pattern, indicating that

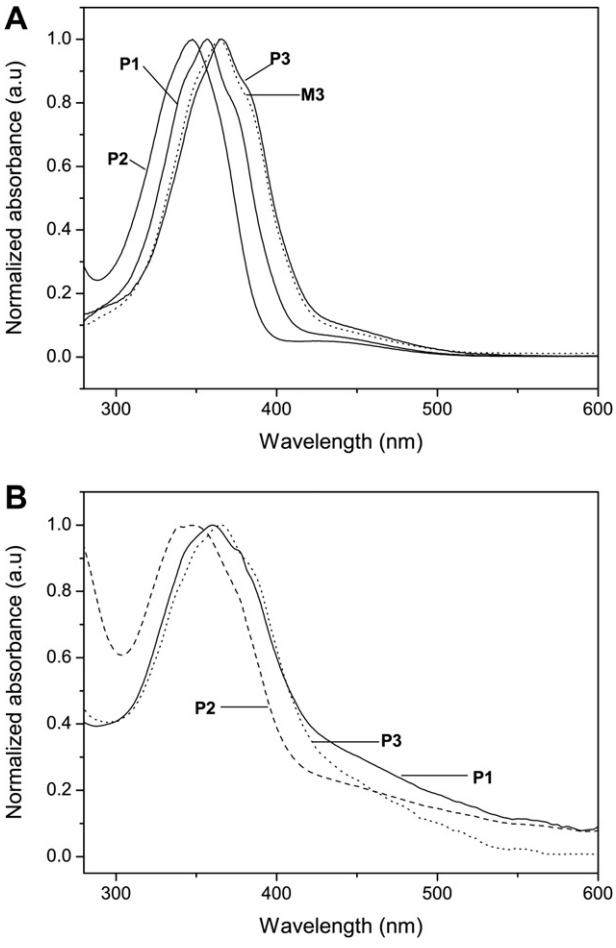

Fig. 5. A) Normalized absorption spectra of **M3** and **P1**–**P3** in THF. B) Normalized absorption spectra of **P1**, **P2** and **P3** in film.

introduction of the silsesquioxane moeity has no significant effect on the electronic structure of organic chromophores [34]. **P1**–**P3** show strong absorption peaks located at 356, 347, and 365 nm, respectively, which are assigned to the π–π* electronic transitions of the corresponding conjugated azobenzene chromophores. The maximum absorption peak of **P2** showed 9 nm blue shifts compared with that of **P1**, which may result from the rigid spacer –PhCOO-group twisting the planar azobenzene group. When terminal methoxyl group was replaced with acylamido group containing long chain, the maximum absorption peak of **P3** shows 8 nm red shifts in comparison with that of **P1**, which may be due to a more regular arrangement of the molecules induced by the hydrogen band between acylamido groups in **P3** [35]. Simultaneously, it is found that all the hybrids exhibit good film-forming properties. Fig. 5B displays the absorption spectra of **P1**, **P2** and **P3** in films. They are similar to the absorption spectra in dilute solutions, with the absorption maxima at 360, 347 and 366 nm, respectively. The similarity between the film and the dilute solution spectra suggests the star-type structure in hybrids significantly refrain from aggregation effect of azobenzene chromophore in the solid state [36].

3.3. Thermal properties

Thermal stability of optical limiting materials is one of the most important aspects for improvement of device lifetime and reliability. The thermal properties of hybrids were evaluated by TGA and DSC. Although $\mathbf{T_8^H}$ and all the monomers are crystalline solids with distinct melting points, there is no sign of melting or crystallization and glass transition of the resulting hybrid up to the decomposition point (see the example curves shown in Fig. 6A). The amorphous character may result from star-like structure with the rigid azobenzene chromophore moieties projecting off the spherical POSS core in three dimensions, thus minimizing intra or inter π–π interactions [37] and effectively preventing intermolecular regular stacking resulting from joule heating during device operation [19]. Fig. 6B depicts the TGA curves of all hybrid materials under nitrogen at a heating rate of 10 °C/min. The thermal decomposition temperatures (T_d, 5 wt% loss) of monomer **M1**, **M2** and **M3** are at 262, 272, and 280 °C, respectively. However, the resultant hybrids exhibit T_d at 295, 319 and 321 °C for **P1**, **P2**, and **P3**, respectively, hinting that the incorporation of inorganic POSS into organic NLO chromophores effectivly enhances the thermal stability of the resulting founctinal hybrids.

3.4. Optical limiting properties

Fig. 7 shows the optical limiting performances of **P1** (concentration $c = 1.63$ mg/mL), **P2** ($c = 1.07$ mg/mL), and **P3** ($c = 1.02$ mg/mL) at the same linear transmittance ($T = 73\%$) to 532 nm laser pulses in THF. At low incident energies the optical responses follow Beer's law. Deviations from Beer's law at higher energies indicate the occurrence of optical limiting. Experiments with THF solvent alone afforded no detectable OL effect. This indicates that the solvent contribution is negligible. As seen in Fig. 7, the limiting threshold (incident fluence at which the output fluence starts to deviate from linearity) and amplitude (maximum output fluence) of **P1** are 0.76 and 0.92 J/cm^2 and those of **P2** are 0.65 and 0.84 J/cm^2, respectively. In comparison with **P1** and **P2**, **P3** showed a little better optical limiting performance, the limiting threshold and amplitude are 0.51 and 0.78 J/cm^2, respectively. Simultaneously, the OL properties of the monomers in THF at the same transmittance were also measured. Typical example of OL performance of **M2** is shown in Fig. 7. It was found that the OL properties of the hybrids were not significantly difference from those of corresponding monomers, indicating that incorporation the

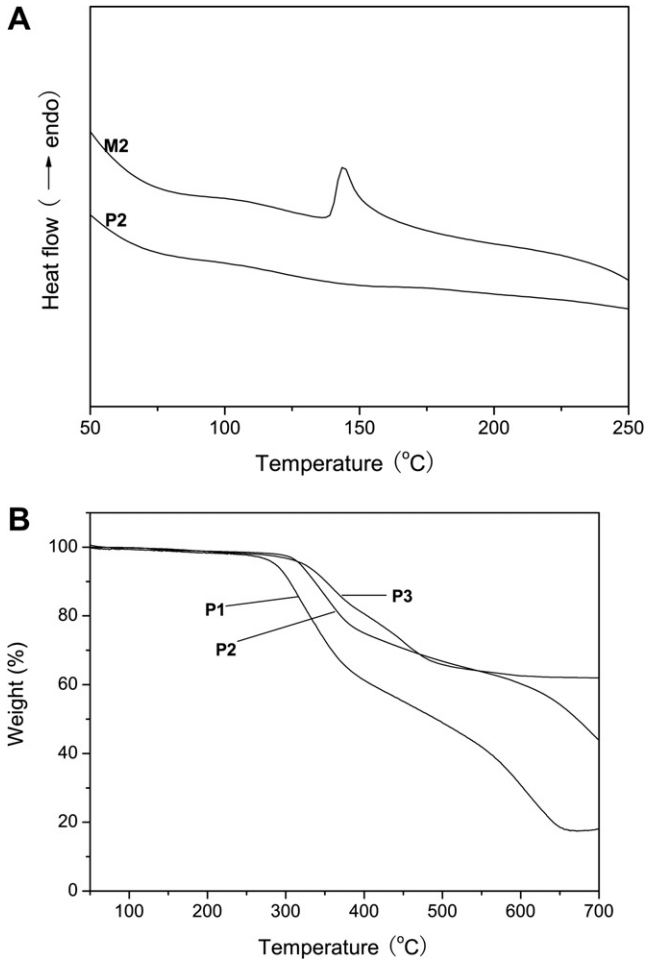

Fig. 6. A) DSC curves of **M2** and **P2**. B) TGA thermograms of **P1**–**P3** at a ramp rate of 10 °C/min in nitrogen flow.

silsesquioxane core onto the NLO chromophore has no significant effects on the electronic structures of the chromophoric group, which is consistent with the result of UV–vis absorption spectra. For detecting the photostability of these hybrid materials, we also measured the UV absorption spectra of the hybrid solutions before and after the laser irradiation and no measurable difference were observed, showing that the hybrids possess good photostability.

Fig. 8 shows the optical limiting performances of **P3** in THF with different concentrations. It can be found that the limiting effect was affected by concentration, with higher concentration solutions exhibiting better performances. For example, the concentration of **P3** is 0.87 mg/mL ($T = 83\%$), the optical limiting performance was faintly. When the concentration increases from 1.02 ($T = 73\%$) to 1.98 mg/mL ($T = 54\%$), the limiting threshold of the sample varies from 0.51 to 0.40 J/cm^2 and the limiting amplitude varied from 0.78 to 0.51 J/cm^2, respectively. Similar results were also found in our previous works [10]. It is the reason that the solution with a high concentration has more molecules per unit volume, which should absorb the energy of the harsh laser more efficiently.

The optical limiting mechanisms of organic compounds can be two-photon absorption (TPA) or reverse saturable absorption (RSA). Generally, TPA can be yielded in principle under the laser irradiation of picosecond or shorter pulses. RSA can be achieved on nanosecond or longer pulses, rather than a picosecond time scale, because of the different excited-state lifetimes involved in a multi-level energy process [38]. In this work, the hybrids were excited by the laser with 4 ns pulse width at 532 nm. Therefore, we consider that the optical limiting properties of these hybrids may be mainly originated from RSA of molecules.

The optical limiting property of RSA molecules can be also evaluated by the ratio of the excited-state absorption cross-section (σ_{ex}) to the ground state absorption cross-section (σ_0) of molecules, which was defined as $\sigma_{ex}/\sigma_0 = \ln T_{sat}/\ln T_0$. T_{sat} is the saturated transmittance for high degrees of excitation [39]. The larger the value of σ_{ex}/σ_0 is, the better the optical limiting performance is. In our experimental set up, although we are unable to reach the saturable transmittance for these compounds, we can use the transmittance at 1.5 J/cm^2 to calculate the lowest bound for σ_{ex}/σ_0. Based on the experiment data illustrated in Fig. 7, the calculated values of σ_{ex}/σ_0 for **P1**–**P3** are 1.55, 1.84 and 2.01, respectively, further confirming that their optical limiting mechanisms are mainly originated from reverse saturable absorption resulting from large excitation state absorption cross-section.

3.5. Nonlinear optical properties of the hybrids

The NLO properties of these hybrids **P1**–**P3** were investigated by using the *Z*-scan technique. It can be seen from Fig. 5 that all the hybrids have low absorbance at 532 nm. This promises low intensity

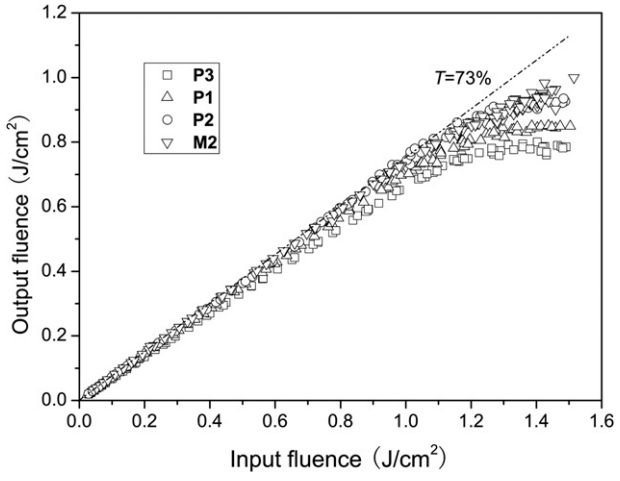

Fig. 7. Optical responses to laser light of **P1**, **P2** and **P3** with the same linear transmission of 73% in THF.

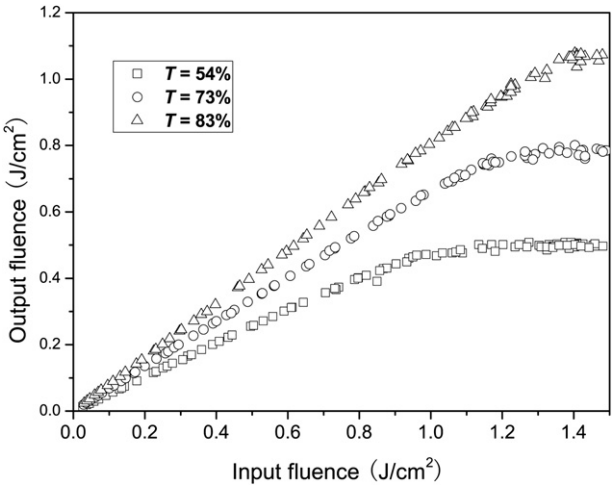

Fig. 8. Optical responses to laser light of **P3** with different linear transmittances in THF.

loss and little temperature change by photon absorption during the NLO measurements. The *Z*-scan result of **P2** is shown in Fig. 9 as a representative example. The nonlinear absorption performance is evaluated under an open aperture configuration. Theoretical curves of transmittance against the *z*-position based on equations (1) and (2), are fitted to the observed *Z*-scan data by varying the effective third-order nonlinear absorption coefficient β value [32].

$$T(z,s=1)=\sum_{m=0}^{\infty}\frac{[-q_0(z)]^m}{(m+1)^{3/2}},\quad \text{for}\quad |q_0|<1 \tag{1}$$

$$q_0(z)=\beta I_0(t)L_{\text{eff}}/\left(1+z^2/z_0^2\right) \tag{2}$$

Where β is the nonlinear absorption coefficient, $I_0(t)$ the intensity of laser beam at focus ($z=0$), $L_{\text{eff}}=[1-\exp(-\alpha_0 L)]/\alpha_0$ is the effective thickness with α_0 the linear absorption coefficient and L the sample thickness, z_0 is the diffraction length of the beam, and z is the sample position. The solid line in Fig. 9a is theoretical curve from equations (1) and (2). Thus, β of the hybrids can be determined through the fitting of the experimental data with the equations.

The nonlinear refractive property of **P2** was assessed by dividing the normalized *Z*-scan data obtained in the close aperture configuration by those obtained in the open aperture configuration (Fig. 9b). The effective third-order nonlinear refractive index n_2 can be derived from the difference between normalized transmittance values at valley and peak positions (ΔT_{v-p}) by using equation (3) [32]:

$$n_2=\frac{\lambda\alpha_0}{0.812\pi I_0(1-e^{-\alpha_0 L})\cdot(1-S)^{0.25}}\cdot\Delta T_{v-p} \tag{3}$$

Where S is the aperture size ($S=0.18$). Thus, the nonlinear refractive coefficients of the hybrids can be determined with equation (3). In accordance with the observed β and n_2 values, the third-order susceptibility $\chi^{(3)}$ value can be calculated with the following equation [32]:

$$|\chi^{(3)}|=\sqrt{\left|\frac{cn_0^2}{80\pi}\cdot n_2\right|^2+\left|\frac{9\times10^8\varepsilon_0 n_0^2c^2}{4\pi\omega}\cdot\beta\right|^2} \tag{4}$$

Where ε_0 is the permittivity of vacuum, c the speed of light, n_0 the refractive index of the medium and $\omega=2\pi c/\lambda$. The calculated nonlinear optical coefficients of these composites are summarized in Table 1. From Table 1 it can be seen that these hybrids exhibit

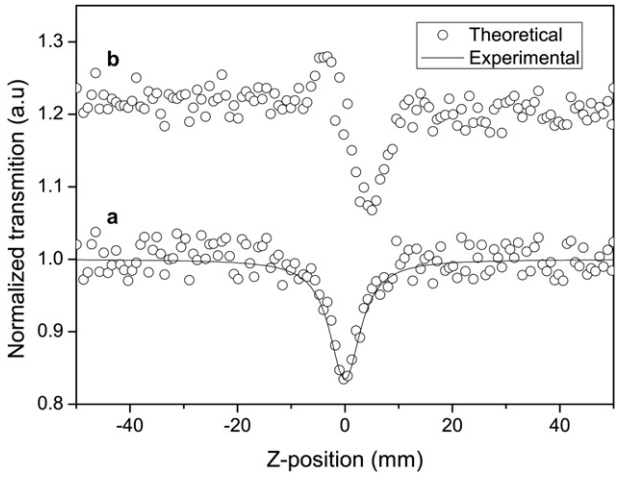

Fig. 9. *Z*-scan data of **P2** in THF.

Table 1
Properties of the **P1**, **P2** and **P3**.

Sample	Limiting threshold (J/cm^2)[a]	Limiting amplitude (J/cm^2)[b]	Nonlinear optical values[c]		
			β (m/W)	n_2 (m^2/W)	$\chi^{(3)}$ (esu)
P1	0.76	0.92	3.88×10^{-11}	7.48×10^{-18}	5.75×10^{-12}
P2	0.65	0.84	5.78×10^{-11}	7.39×10^{-18}	6.91×10^{-12}
P3	0.51	0.78	1.63×10^{-10}	1.06×10^{-17}	9.52×10^{-12}

[a] Incident fluence at which the output fluence starts to deviate from linearity.
[b] Maximum output fluence.
[c] Measured by *Z*-scan technique with an 4 ns Nd:YAG laser system at 1 Hz repetition rate and 532 nm wavelength.

good nonlinear absorption properties with β values of 3.88×10^{-11} m W^{-1} (**P1**), 5.78×10^{-11} m W^{-1} (**P2**) and 1.63×10^{-10} m W^{-1} (**P3**), respectively, which is in agreement with the observations made in the OL experiments. Simultaneously, it is also found from Table 1 that **P3** shows the largest $\chi^{(3)}$ value among the three hybrids, which may be attributed to the enhancement effect of hydrogen bond [35].

4. Conclusions

In this work, a group of azobenzene-containing POSS-based star-like hybrid functional materials are succeededly prepared. The results show that incorporation of azobenzene NLO chromophores into POSS core have endowed the hybrids with good film-forming property and photostability, higher thermal stability, novel optical limiting properties and large $\chi^{(3)}$ susceptability and the optical limiting mechanism is mainly originated from the reverse satuable absorption of molecules. The work provides a novel path for designing new optical limiting materials with high thermal stability and good processability.

Acknowledgement

This research was financially supported by the National Natural Science Fund of China (Grant Nos. 90606011, 50472038 and 20974018), Ph.D. Program Foundation of Ministry of Education of China (No.20070255012), Shanghai Leading Academic Discipline Project (No. B603) and Open Project of The State Key Laboratory of Crystal Materials (KF0809), the Program of Introducing Talents of Discipline to Universities (No.111-2-04) and China Postdoctoral Science Foundation (20080440563 and 200902193).

References

[1] Tutt LW, Kost A. Nature 1992;356:225–6.
[2] Tutt LW, Boggess TF. Progress in Quantum Electronics 1993;17:299–338.
[3] Tang BZ, Xu H, Lam JWY, Lee PPS, Xu K, Sun Q, et al. Chemistry of Materials 2000;12:1446–55.
[4] Ehrlich JE, Wu XL, Lee I-YS, Hu Z-Y, Röckel H, Marder SR, et al. Optics Letters 1997;22:1843–5.
[5] Li Z, Dong Y, Häussler M, Lam JWY, Dong Y, Wu L, et al. Journal of Physical Chemistry B 2006;110:2302–9.
[6] Tang BZ, Xu H. Macromolecules 1999;32:2569–76.
[7] Guang S, Yin S, Xu H, Zhu W, Gao Y, Song Y. Dyes and Pigments 2007;73:285–91.
[8] Yuan WZ, Sun JZ, Liu JZ, Dong Y, Li Z, PengXu H, et al. Journal of Physical Chemistry B 2008;112:8896–905.
[9] Su X, Wu L, Yin S, Xu H, Wu Z, Song Y, et al. Journal of Macromolecular Science, Pure and Applied Chemistry 2007;44:691–7.
[10] Su X, Xu H, Guo Q, Shi G, Yang J, Song Y, et al. Journal of Polymer Science, Part A: Polymer Chemistry 2008;46:4529–41.
[11] Su X, Xu H, Yang J, Lin N, Song Y. Polymer 2008;49:3722–30.
[12] Wang X, Guang S, Xu H, Su X, Yang J, Song Y, et al. Journal of Materials Chemistry 2008;18:4202–9.
[13] Wang X, Wu J, Xu H, Wang P, Tang BZ. Journal of Polymer Science, Part A: Polymer Chemistry 2008;46:2072–83.
[14] Su X, Guang S, Xu H, Liu X, Li S, Wang X, et al. Macromolecules 2009; 42:8969–76.

[15] Lin W-J, Chen W-C, Wu W-C, Niu Y-H, Jen AK-Y. Macromolecules 2004; 37:2335–41.
[16] Mather PT, Jeon HG, Romo-Uribe A, Haddad TS, Lichtenhan JD. Macromolecules 1999;32:1194–203.
[17] Zhang C, Bunning TJ, Laine RM. Chemistry of Materials 2001;13:3653–62.
[18] Markovic E, Clarke S, Matisons J, Simon GP. Macromolecules 2008; 41:1685–92.
[19] Markovic E, Ginic-Markovic M, Clarke S, Matisons J, Hussain M, Simon GP. Macromolecules 2007;40:2694–701.
[20] Lo MY, Zhen C, Lauters M, Jabbour GE, Sellinger A. Journal of The American Chemical Society 2007;129:5808.
[21] Tanaka K, Inafuku K, Adachi S, Chujo Y. Macromolecules 2009;42:3489–92.
[22] Su HW, Chen WC. Materials Chemistry and Physics 2009;114:736–41.
[23] Naga N, Kihara Y, Miyanaga T, Furukawa H. Macromolecules 2009;42: 3454–62.
[24] Xu H, Yang B, Wang J, Guang S, Li C. Journal of Polymer Science, Part A: Polymer Chemistry 2007;45:5308–17.
[25] Yang B, Xu H, Wang J, Gang S, Li C. Journal of Applied Polymer Science 2007;106:320–6.
[26] Xu H, Yang B, Gao X, Li C, Guang S. Journal of Applied Polymer Science 2006;101:3730–5.
[27] Xu H, Yang B, Wang J, Guang S, Li C. Macromolecules 2005;38:10455–60.
[28] Ceyhan T, Yüksek M, Yağlıoğlu HG, Salih B, Erbil MK, Elmalı A, et al. Dalton Transactions; 2008:2407–13.
[29] Su X, Xu H, Deng Y, Li J, Zhang W, Wang P. Materials Letters 2008;62:3818–20.
[30] Agaskar PA. Journal of the American Chemical Society 1989;111:6858–9.
[31] Apfel MA, Finkelmann H, Janini GM, Laub RJ, Luehmann BH, Price A, et al. Analytical Chemistry 1985;57:651–8.
[32] Sheik-Bahae M, Said AA, Stryland EWV. Optics Letters 1989;14:955.
[33] Qu S, Song Y, Du C, Wang Y, Gao Y, Liu S, et al. Optics Communications 2001; 196:317–23.
[34] Xiao S, Nguyen M, Gong X, Cao Y, Wu H, Moses D, et al. Advanced Functional Materials 2003;13:25–9.
[35] Yin S, Xu H, Shi W, Gao Y, Song Y, Tang BZ. Dyes and Pigments 2006; 71:138–44.
[36] Mikroyannidis JA, Gibbons KM, Kulkarni AP, Jenekhe SA. Macromolecules 2008;41:663–74.
[37] Yoonlo M, Ueno K, Tanabe H, Sellinger A. The Chemical Record 2006;6: 157–68.
[38] Sun WF, Bader MM, Carvalho T. Optics Communications 2003;215:185–90.
[39] Perry JW, Mansour K, Marder SR, Perry KJ, Daniel Alvarez J, Choong I. Optics Letters 1994;19:625–7.